Available online at www.sciencedirect.com
ScienceDirect
Ceramics International 37 (2011) 139–144
CERAMICS INTERNATIONAL
www.elsevier.com/locate/ceramint

Microstructural design and elaboration of multiphase ultra-fine ceramics

Paola Palmero *, Valentina Naglieri [1], Giulia Spina, Mariangela Lombardi [2]

Dept. of Materials Science and Chemical Engineering, Politecnico di Torino, INSTM, R.U. PoliTO, LINCE Lab., Corso Duca degli Abruzzi 24, 10129 Torino, Italy

Received 29 May 2010; received in revised form 30 June 2010; accepted 26 July 2010
Available online 21 August 2010

Abstract

Three-phase composites in the system Al_2O_3–YAG–ZrO_2 (AYZ) were produced by doping the surface of commercial alumina nanopowders with inorganic precursors of the second phases. Materials with three different compositions were prepared, in which 5, 20 and 33 vol.% of each second phase were respectively present. Pure crystalline phases were obtained in the final composites, as assessed by X-ray diffraction. Green bodies were produced by slip casting and uniaxial pressing. Subsequent free sintering led to full densification and to highly homogeneous microstructures, in terms of grain size and second phase distribution. A progressive refinement of the alumina matrix grain size was achieved by increasing the second phase content, varying from micro/nano-composites to ultra-fine structures, with a mean grain size of about 500 nm for all the phases. The three materials presented high Vickers hardness values, as a results of the high final density and ultra-fine, homogeneous microstructures.

Keywords: A. Sintering; B. Nanocomposites; Al_2O_3–YAG–ZrO_2; Microstructure

1. Introduction

The design of engineered ceramics has changed from microstructures to nanostructures in the last few years, since improved mechanical properties were proven in nanomaterials [1]. In 1991 Niihara [2] proposed the ceramic nanocomposites, dividing them into inter/intra micro/nano-composites and nano/nano-composites. According to this classification, many inter and intragranular composites have been developed, in both oxide and non-oxide systems [3–7], in which the ultra-fine 2nd phases induce a dramatic reduction of the matrix grain size, due to a *pinning* effect [8]. Beside finer microstructures, their most remarkable advantages are improved fracture strength, toughness and creep resistance [3,9–11].

An enhanced grain growth control can be achieved by the elaboration of the so-called duplex microstructures, which consist of two immiscible phases, contained in similar volume fractions, that can give rise to interconnected structures, so that the growth of each phase is hindered by the other one and long-order interdiffusion is strongly limited [12,13]. Recently, the same approach has been extended to three-phase composites made from immiscible phases, thus to further limit grain growth. A 33 vol.%alumina–33 vol.%YAG–33 vol.%zirconia composite was produced by Kim and Kriven [14], with the aim of yielding materials with high strength retention even after prolonged high temperature annealing. More recently, Oelgardt et al. [15] produced and tested an ultra-fine composite in the same system, with an eutectic composition, with the aim of comparing the basic mechanical properties of their composite to those obtained by directional solidification from eutectic melts.

The challenge in designing such systems is to find at least four immiscible phases, that are distributed in such a way that grains of the same phase are never in contact. Kim et al. produced alumina-based quadruplex and quintuplex composites [16], with the aim of achieving increased microstructural stability during prolonged high-temperature service, due to longer interdiffusion distances between grains of the same phase.

In this paper, three-phase composites in the system Al_2O_3–YAG–ZrO_2, in which zirconia is fully stabilized by yttria (Y-FSZ), were developed. This material is designed for applications in harsh environment and prolonged high-temperature service,

* Corresponding author. Tel.: +39 011 5644678; fax: +39 011 5644699.
E-mail address: paola.palmero@polito.it (P. Palmero).
[1] Now at Materials Sciences Division, MS 62-109, Lawrence Berkeley National Laboratory, Berkeley, CA 94720, United States.
[2] Now at IIT@ POLITO - Centre for Space Human Robotics, C.so Trento 21, 10129 Torino, Italy.

0272-8842/$36.00
doi:10.1016/j.ceramint.2010.08.031

on the ground of the excellent stability of cubic-ZrO_2 over a wide range of temperatures [17] and of the superior creep resistance of YAG [18].

The composite powders were prepared by surface modification of commercial, nanocrystalline alumina powder with inorganic precursors of the second phases, already exploited for the elaboration of biphasic micro/nanocomposites Al_2O_3–5 vol.%ZrO_2 and Al_2O_3–5 vol.%YAG [19]. In the former system, made by two immiscible oxides, tetragonal zirconia directly crystallized on the alumina surface, while the latter is a reactive system in which YAG phase is formed by a solid-state reaction between the yttrium-rich precursor and alumina. In the present work, reactive and non-reactive precursors are both present; in addition, yttrium diffusion and solubilization into zirconia lattice is required to stabilize it in the cubic phase.

The aim of this work is twofold:

(i) to produce three-phase pure materials, in a wide range of 2nd phase volume fraction in the alumina matrix;
(ii) to achieve an effective microstructural tailoring, in terms of second phase distribution and grain size, leading to controlled micro/nano and even nano/nano composite structures.

2. Experimental

A commercial, nanocrystalline transition alumina powder (NanoTek®, supplied by Nanophase Technologies, USA) was used as starting material [20]. NanoTek® aqueous suspensions were dispersed for 3 h by ball-milling, using α-Al_2O_3 spheres (powder/sphere weight ratio of 1/10) and hereafter referred to as A.

Aqueous solutions of $YCl_3.6H_2O$ (Sigma–Aldrich, 99.99% purity) and $ZrCl_4$ (Fluka, >98% purity) were prepared and dropwise added to the alumina dispersed suspensions, with the aim of developing three compositions, with increasing secondary phase volume fractions. Precisely, 90 vol.%Al_2O_3–5 vol.%YAG–5 vol.%ZrO_2 (AYZ-5), 60 vol.%Al_2O_3–20 vol.%YAG–20 vol.%ZrO_2 (AYZ-20) and 34 vol.%Al_2O_3–33 vol.%YAG–33 vol.%ZrO_2 (AYZ-33) composites were prepared. More details about the elaboration method are reported elsewhere [19,21].

The three doped powders were submitted to simultaneous DTA-TG analyses (Netzsch STA 409C) up to 1400 °C at a heating rate of 10 °C/min, in static air. Then, powders were calcined in a wide temperature range (600–1500 °C, for 1 h) to allow by-products decomposition and to investigate the phase development by X-ray diffraction analysis (Philips PW1710) in the 5–70° 2θ range (step size of 0.05° 2θ, for 5 s).

Prior to sintering, the doped powders were heat treated at 1150 °C for 5 min, with the aim of limiting the residual mass loss during firing and inducing the second phases crystallization. However, to limit agglomeration during calcination, such treatments were carried out by instantaneously plunging the powders for few minutes in a tubular furnace kept at the aforementioned temperature (“fast heating”).

Aqueous suspensions of the pre-treated powders (with solid load of 65 wt.%) were dispersed by ball-milling (weight ratio powder/α-Al_2O_3 spheres of 1/5) for a time ranging between 48 and 190 h. De-agglomeration as a function of the dispersion time was followed by laser granulometry (Fritsch model Analysette 22 Compact). The dispersed slurries were then slip cast into porous molds; drying was performed in a humidity-controlled chamber for about 1 week. Aliquots of the dispersed suspensions were also dried and uniaxially pressed in bar at 300 MPa.

Powders sinterability was investigated by absolute dilatometry (Netzsch 402E) up to 1500 °C, by employing a thermal cycle already set up in a previous work [22].

The final density of the composites was determined by Archimedes’s method and referred to the respective theoretical density (TD), calculated by the rule of mixture, assuming values of 3.99 g/cm^3 (JCPDS file n° 46-1212), 4.55 g/cm^3 (JCPDS file n° 33-0040) and 5.82 g/cm^3 (JCPDS file n° 77-2112) for α-alumina, YAG and c-ZrO_2, respectively. Precisely, TD of 4.11, 4.47 and 4.78 g/cm^3 were calculated for AZY-5, AZY-20 and AZY-33, respectively.

The fired microstructures were submitted to SEM characterization (Hitachi S2300), performed on polished and thermally etched surfaces.

Hardness was measured on the polished surface by Vickers indentation, with a load of 1 kg, for 15 s. Al least, 10 measurements were made for each material.

3. Results and discussion

As-received NanoTek® powder is made of ultra-fine, spherical primary particles (Fig. 1) and presents a significant agglomeration, being the average grain size of about 5 μm. After ball-milling, the mean agglomerate size was reduced to about 0.5 μm, yielding sample A.

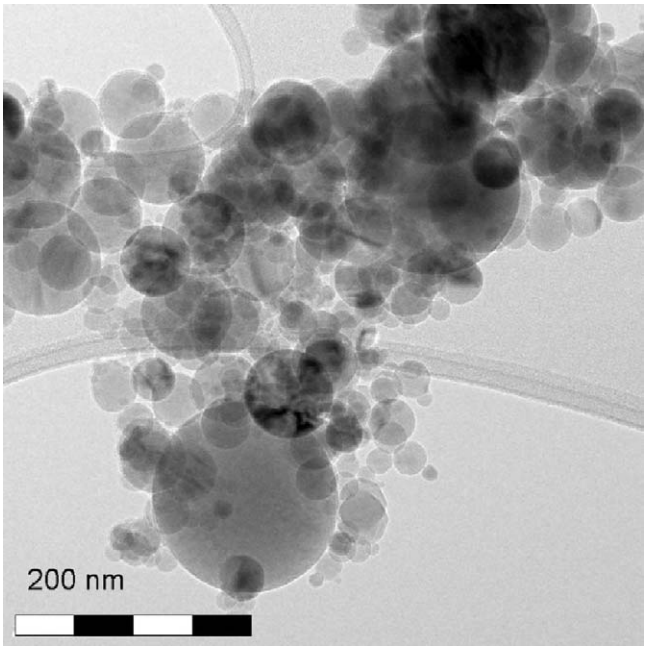

Fig. 1. TEM micrograph of as-received NanoTek®.

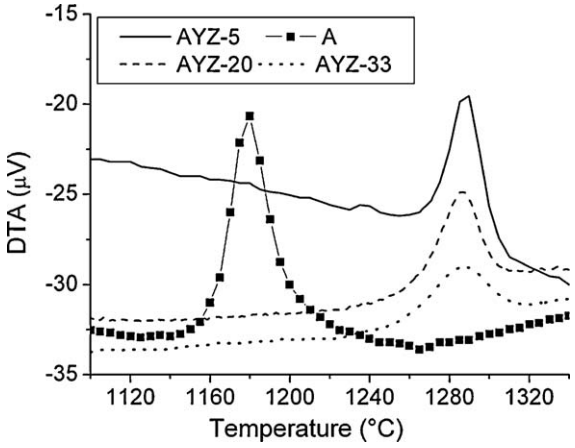

Fig. 2. DTA curves of A and samples AZY-5, AZY-20 and AZY-33.

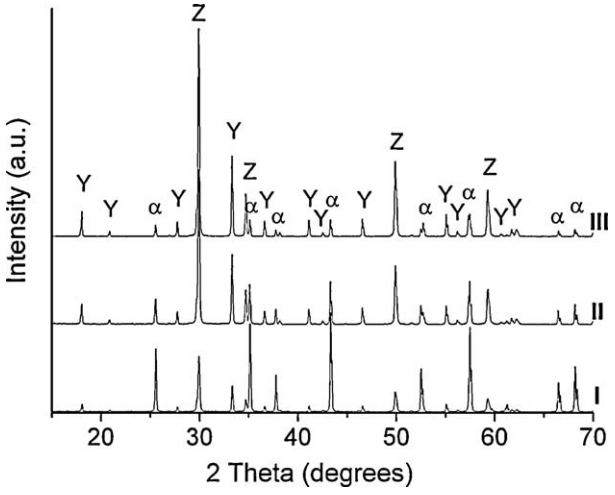

Fig. 3. XRD patterns of AZY-5 (curve I), AZY-20 (curve II) and AZY-33 (curve III) calcined at 1500 °C for 1 h.

TG analyses show that the three doped powders undergo to significant mass loss up to 700 °C, imputable to dehydration as well as to decomposition of organic by-products, such as citric acid and citrate metal complex [21]. Precisely, mass loss of about 33, 60 and 65% were determined for AZY-5, AZY-20 and AZY-33, respectively.

Fig. 2 collects the DTA curves in the high temperature range for sample A and for the three composites. The peak corresponding to the α-alumina crystallization is detected at 1180 °C for pure alumina and at about 1290 °C for the composite powders. As expected on the ground of literature [23], the presence of dopants delays the α-alumina crystallization, but such delay seems to be independent of the second phase amount.

The crystallization path of the three composite powders was followed by performing low and high-temperature treatments. XRD analyses performed on powders calcined at 600 °C for 1 h evidenced the formation of cubic $Zr_{0.72}Y_{0.28}O_{1.862}$ (JCPDS file n° 77-2112), near transition aluminas, for all the three powders.

Yttrium aluminates, indeed, start to crystallize at 1200 °C. At this temperature, in fact, the metastable hexagonal phase $YAlO_3$ [JCPDS file n° 74-1334] was detected in all the three compositions, along with traces of YAG [JCPDS file n° 33-0040] in AZY-20 and of both YAG and perovskite $YAlO_3$ phase [JCPDS file n° 33-0041] in AZY-33. At 1300 °C, perovskite and YAG were detected in AZY-5 and AZY-33, while pure YAG was present in AZY-20. Finally, at 1500 °C, all the undesired second phases disappeared: pure α-Al_2O_3, cubic ZrO_2 and YAG were detected in the three composites, as shown in Fig. 3. Fig. 4 shows, indeed, the effectiveness of the "fast heating" for AZY-33; by applying the Scherrer's equation, crystallite size of 16 and 31 nm were respectively determined for the fast and conventionally heated powders.

Dilatometric analysis carried out on pressed sample A, shows that it is characterized by a two-step linear shrinkage [24]. As detailed in a previous paper [22], sample A starts to shrink (T_{onset}) at about 1020 °C, while its maximum transformation rate into α-phase (T_{transf}) occurs at about 1060 °C. Finally, the maximum sintering rate (T_{sint}) of the transformed α-Al_2O_3 is detected at about 1420 °C. The same two-step behavior is presented by pressed AZY-5 sample; however it is characterized by higher T_{onset} and T_{transf} as compared to sample A, thus confirming the role of the dopants in delaying the α-alumina crystallization temperature [25,26]. In addition, AZY-5 exhibits a slightly lower T_{sint} than A, and also a higher densification rate in the second step. For the sake of clarity, T_{onset}, T_{transf} and T_{sint} values of pressed A and AZY-5 are collected in Table 1. Similar green densities (of about 50–52% TD) characterized the two materials, but the composite sample underwent a higher overall linear shrinkage (of about 21%) as compared to A, yielding an almost fully dense material.

The SEM microstructures of pressed A and AZY-5 samples are compared in Fig. 5. Sample A is characterized by a bimodal alumina grain size distribution, since near well-facetted grains of about 1.5–2 μm, abnormally grown particles can be also observed. In addition, a residual, fine porosity can be detected, located in both inter and intra-granular position. In contrast, AZY-5 presents a highly dense microstructure and a narrow alumina grain size distribution, in the range 1–1.5 μm. In

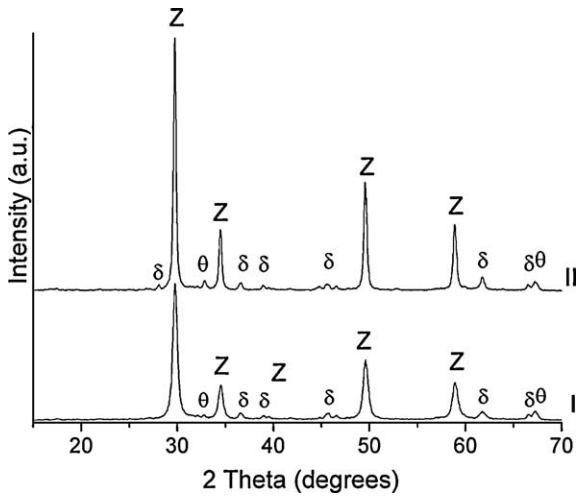

Fig. 4. XRD patterns of AYZ-33 calcined at 1150 °C for 5 min by "fast heating" treatment (curve I) and conventional calcination (curve II).

Table 1
T_{onset}, T_{transf}, T_{sint} and fired density for A and for the pressed (P) and slip cast (SC) samples; Vickers Hardness of slip cast AZY-5, AZY-20 and AZY-33 materials.

Sample	T_{onset} (°C)	T_{transf} (°C)	T_{sint} (°C)	Fired density (%TD)	Hardness (HV)
P A	1020	1060	1420	97.0	–
P AZY-5	1125	1165	1390	99.8	–
SC AZY-5	1120	1160	1385	99.7	1947 ± 46
SC AZY-20	1105	1155	1410	99.3	1797 ± 79
SC AZY-33	1075	1165	1410	98.0	1654 ± 59

addition, the 2nd phases were homogeneously distributed into the matrix, mainly located at the alumina grain boundaries, so able to exert an effective *pinning* on the matrix. In spite of its high final density, some large defects, probably imputable to the pressing procedure, were sometimes observed. Reliability of the fired materials was improved in slip cast bodies, as described below. In Fig. 6, the dilatometric curves of slip cast AZY-5, AZY-20 and AZY-33 are compared. Green values were similar (about 45% TD), but slightly lower than those of the respective pressed materials. In spite of this, very high final densities were achieved: AZY-5 and AZY-20 reached full densification, while a value of 98% TD was obtained by AZY-33 (Table 1). T_{onset} decreased while increasing the 2nd phases amount. AZY-33 started to shrink at about 1075 °C, probably due to yttrium aluminates crystallization. In contrast, T_{transf} seemed to be unaffected by the 2nd phase content, in a good agreement with DTA data. Finally, a slight increase of T_{sint} values (of about 25 °C) from AZY-5 to samples AZY-20 and AZY-33 was recorded (Table 1). The three samples also differ in total linear shrinkage, since values of 25.5%, 25.9% and 23.8% were respectively recorded for AZY-5, AZY-20 and AZY-33.

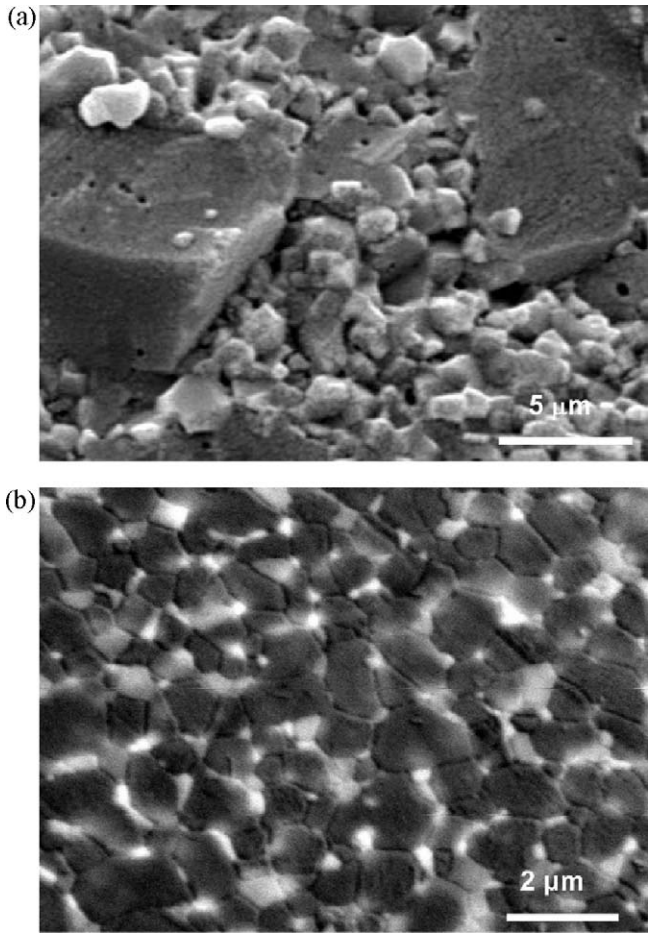

Fig. 5. SEM micrographs of pressed (a) A (SE image) and (b) AZY-5 (BSE image).

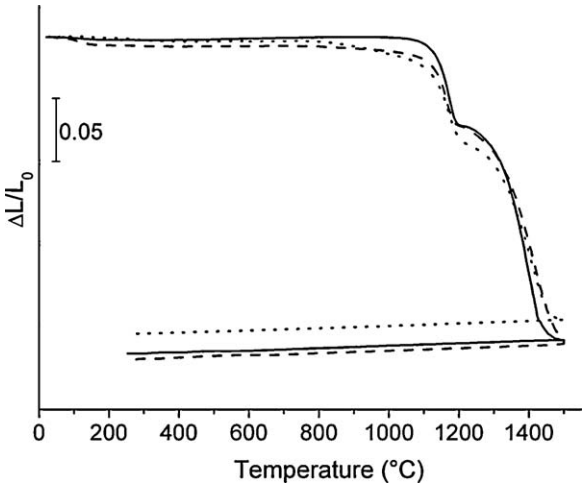

Fig. 6. Dilatometric curves of slip cast AZY-5 (solid line), AZY-20 (dotted line) and AZY-33 (dashed line).

Slip casting allowed the production of defect-free samples. In Fig. 7, the SEM micrographs of AZY-5, AZY-20 and AZY-33 are compared. In all three cases, highly dense and homogeneous microstructures were yielded. In addition, by increasing the 2nd phases content, a progressive refinement of the overall microstructure was achieved. In AZY-5, a micro/nanostructure was produced, in which facetted alumina grains with average size of 1.7 μm were determined, while YAG and ZrO_2 grains were respectively of about 550 and 300 nm. In this sample, second phases were mainly located at alumina grain boundaries, although some intra-granular grains were observed (see arrows in Fig. 7(a)). In AZY-20, a significant reduction of the alumina grain size was observed: in fact, its average value ranged between 1.5 μm and 600 nm, while YAG and zirconia grain sizes were again about 550 and 300 nm, respectively. In AZY-33, a further refinement of alumina was reached, so that an overall mean size of about 500 nm was achieved. The adopted processing method allows an effective microstructural tailoring as well as a progressive refinement of the alumina grain size: as a result, the obtained microstructures well approach the Niihara's micro/nano and nano/nanocomposites models [2], as shown in the insert of Fig. 7(a) and (c).

Even if it was not the major aim of this work, a preliminary mechanical characterization was performed, to get a general overview of the influence of the obtained microstructures on the mechanical behavior. Hardness values of the slip cast samples, as found by Vickers indentation, are summarized in Table 1: they are

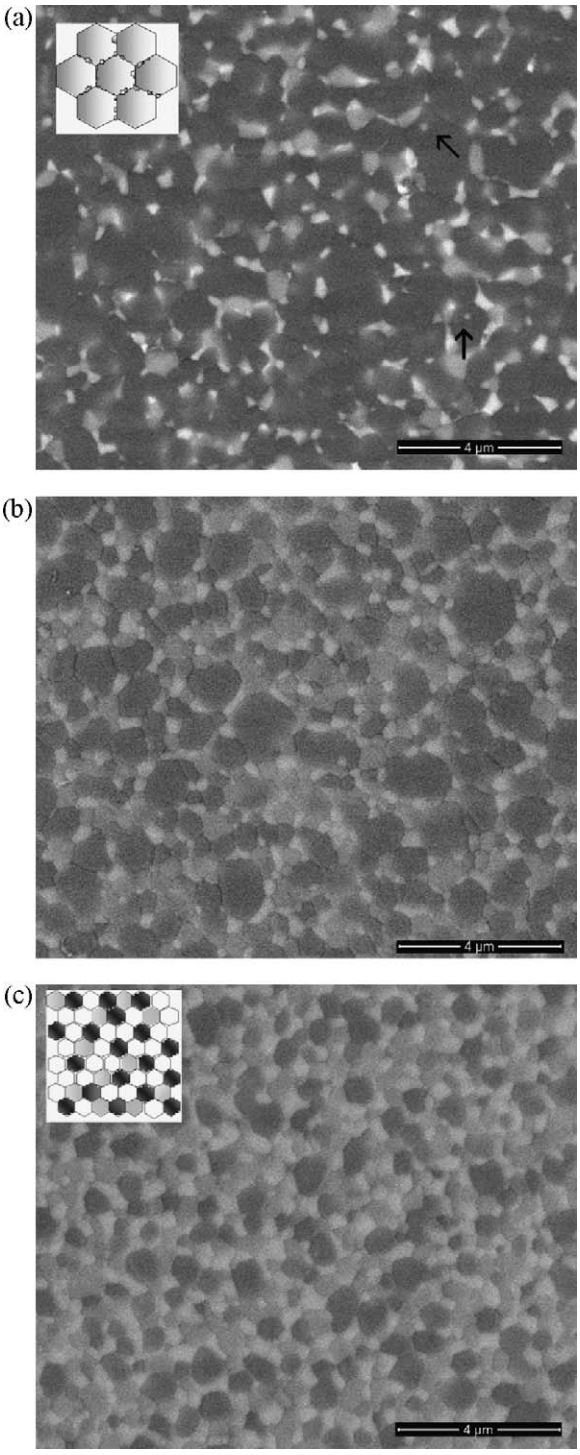

Fig. 7. BSE-SEM micrographs of slip cast (a) AZY-5, (b) AZY-20 and (c) AZY-33, free-sintered at 1500 °C for 3 h. Grains colour in the image: dark gray alumina, light gray YAG, white ZrO_2.

in good agreement with those previously evaluated [15]. In addition, the obtained values are, on average, higher than those usually observed for sintered α-alumina [27], such increment being reasonably due to the very fine microstructures of the produced materials. By comparing the three composites, the higher value was found for AZY-5, as expected on the ground of its higher alumina content, being alumina harder then both YAG

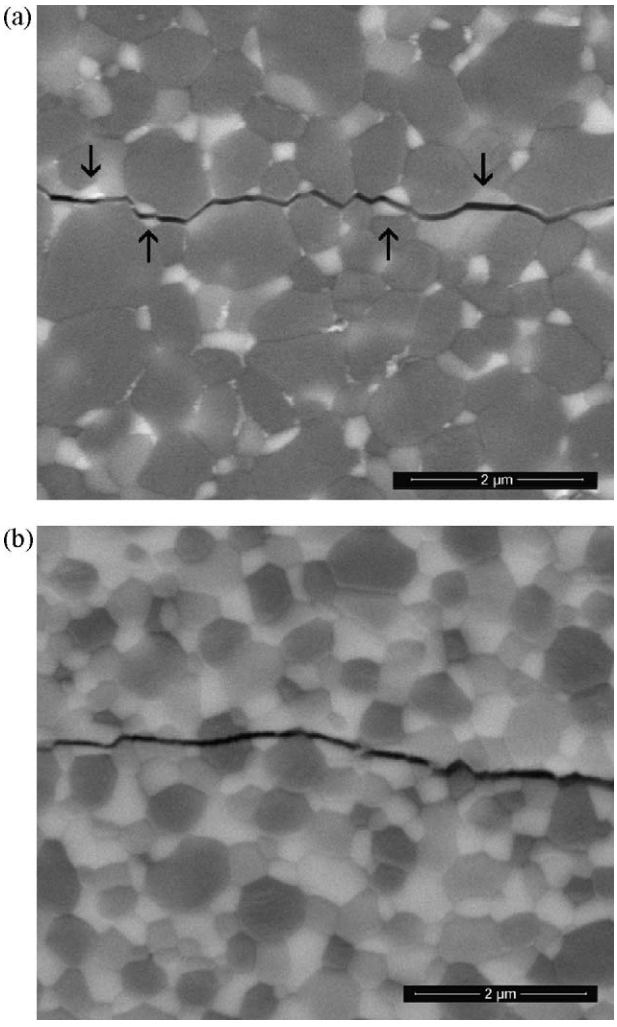

Fig. 8. SEM images of fracture paths in (a) AZY90 and (b) AZY33 indented materials.

[28] and cubic zirconia [29]. AZY-20 was also characterized by a fairly good hardness, due to its very fine microstructure. On the contrary, the lower hardness of AZY-33 can be imputed to its slightly lower final density.

Crack paths of the indented materials were observed by SEM. It is challenging to reach conclusive statements, as both transgranular and intragranular fracture paths are observed in the three samples, as already observed by Oelgardt et al. [15]. Fig. 8(a) shows the fracture path in AZY-5: in this material, intergranular cracks mostly propagate along the alumina grain boundaries. However, if YAG or ZrO_2 grains are placed on the crack path, the fracture preferentially propagate into such phases (see arrows in the figure), instead than through the matrix grains. These observations are in agreement with the strengthening effect of the second phases on alumina grain boundaries and are supported by the behavior observed in AZY-33. In fact, in this material (Fig. 8(b)) cracks even more frequently propagate through the grains, regardless form the considered phase. A systematic mechanical investigation is therefore in progress in order to better state the relationship between microstructural features and mechanical data.

4. Conclusions

This paper deals with the exploitation of an innovative process for the elaboration of multiphase ceramic composites, which consists in doping commercial, nanocrystalline alumina powders with aqueous solutions of both yttrium and zirconium chlorides, to develop alumina–YAG–cubic zirconia composites. The dopant amount was progressively increased, to obtain the three following compositions: 90 vol.%Al_2O_3–5 vol.%YAG–5 vol.%ZrO_2 (AYZ-5), 60 vol.%Al_2O_3–20 vol.%YAG–20 vol.%ZrO_2 (AYZ-20) and 34 vol.%Al_2O_3–33 vol.%YAG–33 vol.%ZrO_2 (AYZ-33). After calcination at high-temperature, pure tri-phased powders were produced, in all the three cases.

By pressureless sintering slip cast green bodies, almost fully dense composites were obtained, presenting a homogeneous distribution of YAG and ZrO_2 grains in the alumina matrix. The second phase grains were able to exert an effective *pinning* on the alumina grain boundaries, strongly limiting grain growth. In addition, a progressive refinement of the alumina matrix was produced by passing from composition AZY-5 to AZY-33. In the former case, a micro-nanocomposite was produced; in the latter, an ultra-fine microstructure was yielded, with an average grain size of about 500 nm.

Vickers tests allowed to assess good hardness values for the three materials, especially for AZY-5, in which the highest alumina content was coupled to a homogeneous and very fine microstructure.

References

[1] H. Gleiter, Nanostructured materials: state of the art and perspectives, Nanostruct. Mater. 6 (1995) 3–14.

[2] K. Niihara, New design concept of structural ‘‘ceramic nanocomposites’’, The Centennial Memorial Issue of the Ceramic Society of Japan 99 (1991) 974–982.

[3] R. Torrecillas, M. Schehl, L.A. Diaz, J.L. Menendez, J.S. Moya, Creep behavior of alumina/YAG nanocomposites obtained by a colloidal processing route, J. Eur. Ceram. Soc. 27 (2007) 143–150.

[4] J. Chandradass, J.H. Yoon, D.S. Bae, Synthesis and characterization of zirconia doped alumina nanopowder by citrate–nitrate process, Mater. Sci. Eng. A 473 (2008) 360–364.

[5] J.H. Zhao, L.C. Stearns, M.P. Harmer, H.M. Chan, G.A. Miller, Mechanical-behavior of alumina silicon-carbide nanocomposites, J. Eur. Ceram. Soc. 76 (1993) 503–510.

[6] A. Nakahira, K. Niihara, J. Ohkijima, T. Hirai, Al_2O_3/Si_3N_4 nano-composites, J. Jpn. Soc. Powd. Powd. Metal. 36 (1989) 239–242.

[7] J.D. Kuntz, G.D. Zhan, A.K. Mukherjee, Nanocrystalline-matrix ceramic composites for improved fracture toughness, MRS Bull. 29 (2004) 22–27.

[8] L.C. Stearns, M.P. Harmer, Particle-inhibited grain growth in Al_2O_3–SiC. I. Experimental results, J. Am. Ceram. Soc. 79 (1996) 3013–3019.

[9] A. Bellosi, D. Sciti, S. Guicciardi, Synergy and competition in nano- and micro-design of structural ceramics, J. Eur. Ceram. Soc. 24 (2004) 3295–3302.

[10] Y.K. Jeong, K. Niihara, Microstructure and mechanical properties of pressureless sintered Al_2O_3/SiC nanocomposites, Nanostruct. Mater. 9 (1997) 193–196.

[11] R.H.J. Hannink, P.M. Kelly, B.C. Muddle, Transformation toughening in zirconia-containing ceramics, J. Am. Ceram. Soc. 83 (2000) 461–487.

[12] J.D. French, M.P. Harmer, H.M. Chan, G.A. Miller, Coarsening resistant dual-phase interpenetrating microstructures, J. Am. Ceram. Soc. 73 (1990) 2508–2510.

[13] S.J. Le, W.M. Kriven, A sub-micron scale duplex zirconia and alumina composites by polymer complexation processing, Ceram. Eng. Sci. Proc. 20 (1999) 69–76.

[14] D.K. Kim, W.M. Kriven, Processing and characterization of multiphase ceramic composites. Part II. Triplex composites with a wide sintering temperature range, J. Am. Ceram. Soc. 91 (2008) 793–798.

[15] C. Oelgardt, J. Anderson, J.G. Heinrich, G.L. Messing, Sintering, microstructure and mechanical properties of Al_2O_3–Y_2O_3–ZrO_2 (AYZ) eutectic composition ceramic microcomposites, J. Eur. Ceram. Soc. 30 (2010) 649–656.

[16] D.K. Kim, W.M. Kriven, Processing and characterization of multiphase ceramic composites. Part III. Strong, hard and tough, high temperature-stable quadruplex and quintuplex composites, J. Am. Ceram. Soc. 91 (2008) 799–805.

[17] T. Chen, S. Tekeli, R.P. Dillon, M.L. Mecartney, Phase stability, microstructural evolution and room temperature mechanical properties of TiO_2 doped 8 mol% Y_2O_3 stabilized ZrO_2 (8Y-CSZ), Ceram. Int. 34 (2008) 365–370.

[18] T.A. Parthasarathy, T.I. Mah, K. Keller, Creep mechanism of polycrystalline yttrium aluminum garnet, J. Am. Ceram. Soc. 75 (1992) 1756–1759.

[19] P. Palmero, V. Naglieri, J. Chevalier, G. Fantozzi, L. Montanaro, Alumina-based nanocomposites obtained by doping with inorganic salt solutions: application to immiscible and reactive systems, J. Eur. Ceram. Soc. 29 (2009) 59–66.

[20] http://www.nanophase.com.

[21] V. Naglieri, P. Palmero, L. Montanaro, Preparation and characterization of alumina-doped powders from the design of multi-phasic nano-micro composites, J. Therm. Anal. Calorim. 97 (2009) 231–237.

[22] P. Palmero, M. Lombardi, L. Montanaro, M. Azar, J. Chevalier, V. Garnier, G. Fantozzi, Effect of heating rate on phase and microstructural evolution during pressureless sintering of a nanostructured transition alumina, Int. J. Appl. Ceram. Technol. 6 (2009) 420–430.

[23] P. Bowen, C. Carry, H. Hofmann, C. Legros, Phase transformation and sintering of γ-Al_2O_3: effect of powder characteristics and dopants (Mg or Y), Key Eng. Mater. 132 (1997) 904–907.

[24] C. Legros, C. Carry, P. Bowen, H. Hofmann, Sintering of a transition alumina: effects of phase transformation, powder characteristics and thermal cycle, J. Eur. Ceram. Soc. 19 (1999) 1967–1978.

[25] R. Voytovych, I. MacLaren, M.A. Gülgün, R.M. Cannon, M. Rühle, The effect of yttrium on densification and grain growth in alpha-alumina, Acta Mater. 50 (2002) 3453–3463.

[26] F.F. Lange, M.M. Hirlinger, Hindrance of grain growth in Al_2O_3 by ZrO_2 inclusions, J. Am. Ceram. Soc. 67 (1984) 164–168.

[27] R.G. Munro, Evaluated material properties for a sintered α-alumina, J. Am. Ceram. Soc. 80 (1997) 1919–1928.

[28] J. Li, Y.S. Wu, Y.B. Pan, W.B. Liu, L.P. Huang, J.K. Guo, Fabrication, microstructure and properties of highly transparent Nd:YAG laser ceramics, Opt. Mater. 31 (2008) 6–17.

[29] A.H De Aza, J. Chevalier, G. Fantozzi, M. Schehl, R. Torrecillas, Crack growth resistance of alumina, zirconia and zirconia toughened alumina ceramics for joint prostheses, Biomaterials 23 (2002) 937–946.